PROCEEDINGS OF SCIENCE

Highlight of LHAASO science results on PeVatrons

Sha Wu[a,b,*] **and Songzhan Chen**[a,b] **on behalf of the LHAASO Collaboration**

[a] *Key Laboratory of Particle Astrophysics, Institute of High Energy Physics, Chinese Academy of Sciences, 100049 Beijing, China*

[b] *TIANFU Cosmic Ray Research Center, Chengdu, Sichuan, China*

E-mail: wusha@ihep.ac.cn

The observation of ultra-high energy (UHE, E>100 TeV) gamma-ray sources plays a crucial role in identifying Galactic PeV accelerators, also known as PeVatrons. The Large High Altitude Air Shower Observatory (LHAASO) is a large hybrid extensive air shower array, constructed at Haizi Mountain, 4410 m a.s.l., in China. With its wide field of view and high sensitivity, LHAASO is an ideal instrument for the detection and study of PeVatrons within our Galaxy. Since July 2021, the whole LHAASO detector array has been completed and operated in good states. Through an all-sky survey, we have observed ultra-high energy gamma-ray emissions in 43 regions associated with pulsars, supernova remnants (SNR), young star clusters, and other celestial objects. In this proceeding, we will present the results obtained from representative gamma-ray sources and discuss our observations of diffuse gamma-ray emissions along the Galactic plane.

38th International Cosmic Ray Conference (ICRC2023)
26 July - 3 August, 2023
Nagoya, Japan

*Speaker

PoS(ICRC2023)010

1. Introduction

Cosmic rays (CRs) exhibit an almost power-law energy spectrum from 10^9 eV to 10^{20} eV. It is widely believed that CRs with energies up to a few PeV (the "knee") originate from accelerators within Galaxy. Due to the deflection caused by the Galactic magnetic field, the arrival direction of CRs at Earth does not directly point back to their sources. However, gamma-rays, prodeced by relativistic protons interacting with the surrounding medium near the accelerators, can be used to investigate the origin of CRs. The typical energy of gamma rays relative to parent CRs is about $1/10$ [1]. Therefore, the detection of UHE gamma-rays is crucial to the identification of PeVatrons.

In recent years, extensive air shower arrays have detected gamma-ray emissions with energy above 100 TeV. The first UHE source, the Crab Nebula, was observed and reported by Tibet ASγ in 2019[2]. Subsequently, four additional UHE sources were revealed by the Tibet ASγ and HAWC [3]. With a sensitivity of approximately 1% Crab unit to gamma ray sources, LHAASO can survey the northern sky with full duty cycle and a large field of view, corresponding to almost 2/3 of the celestial sphere [4]. In 2021, the LHAASO half-array reported the detection of twelve UHE gamma-ray sources with a statistical significance over 7σ [5]. The photons detected by LHAASO far beyond 100 TeV prove the existence of Galactic PeVatrons. It seems that the Milky Way is full of these particle accelerators. However, no Galactic sources have been firmly identified as proton PeVatrons.

The whole LHAASO array has been in service since July 2021. More data can be used to analyse which could give us a much better overview of UHE gamma-ray sky. In this proceeding, we will first introduce the detectors of LHAASO experiment in section 2. We will present the first LHAASO gamma-ray source catalog which include nearly one hundred gamma-ray sources with tens of new discovery in section 3. Some important measurements on different types of UHE gamma-ray sources and on the Galactic plane diffuse gamma-ray will be shown in section 4 and section 5, respectively.

2. The LHAASO experiment

The LHAASO experiment is a hybrid extensive air shower detector, which is located at an altitude of 4410m a.s.l. in Sichuan province, China [4]. One of the most important scientific objectives of LHAASO is to survey the northern UHE gamma-ray sky to investigate the origin of CRs [6]. It is composed of three detector arrays: the square kilometer array (KM2A), 78,000 m^2 water Cherenkov detector array (WCDA) and 18 wide-field air Cherenkov telescopes array (WFCTA). The layout of LHAASO in shown in Fig1.

The KM2A comprises 5195 electromagnetic particle detectors (EDs) and 1188 muon detectors (MDs). It is primarily designed to observe a significant portion of the northern sky, with the aim of detecting gamma-ray sources at energies exceeding 10 TeV. Each ED consists of 4 plastic scintillation tiles covered by 5-mm-thick lead plates to absorb low-energy charged particles in showers and to convert shower gammas into electron–positron pairs [7]. The embedded wavelength-shifting fibers collect scintillation light generated by charged particles and transmit it to a 1.5-inch photomultiplier tube (PMT). The arrival time and number of the particles recorded by PMT can be used to reconstruct the information on the primary shower, such as direction, core location, and

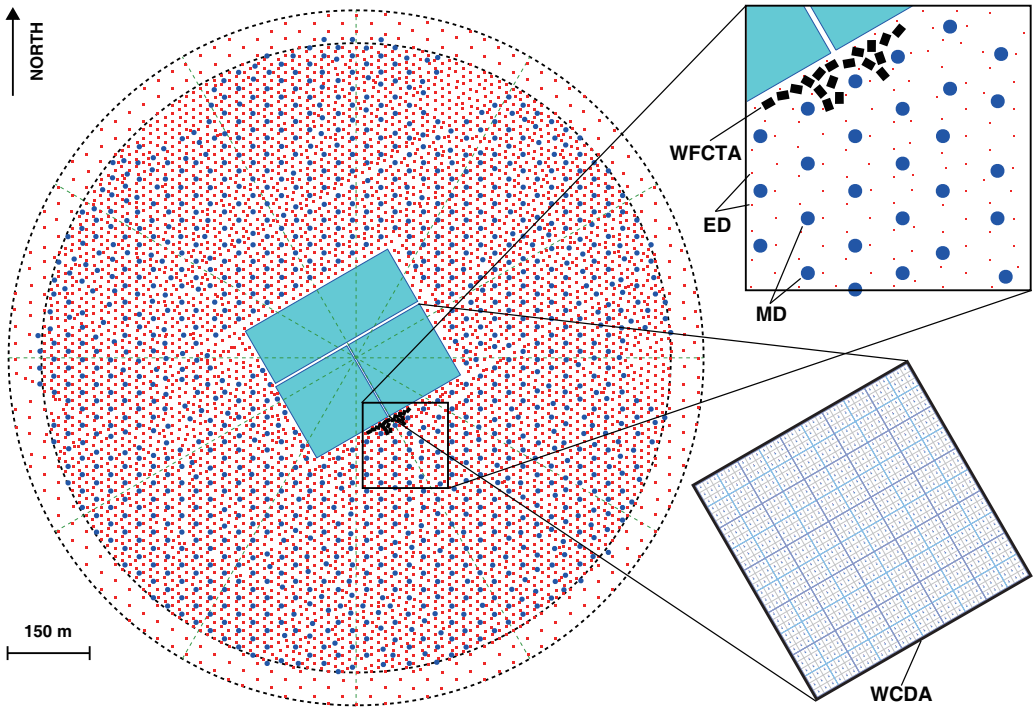

Figure 1: The layout of LHAASO [6].

energy. Each MD includes a water bag with a diameter of 6.8 m and a height of 1.2 m to enclose pure water [8]. The water bag is housed within a cylindrical steel tank, which is buried under 2.5 meters of soil for shielding against high-energy electrons/positrons and photons from showers. At the tank's top center, an 8-inch PMT is installed to collect the Cherenkov light produced by high-energy particles as they traverse through the pure water. The MD array is used to detect mainly the muonic component of showers to discriminate between gamma-ray and hadron induced showers. We conducted a performance study on the KM2A half-array [9]. At 100 TeV, the core resolution of is about 2-4 m, the energy resolution is about 13% and the rejection power is about 4×10^3 for showers at zenith angle below than 20°.

The WCDA is constituted by 3 water ponds, focusing on surveying the northern sky for steady and transient sources from 100 GeV to 20 TeV. Each water pond is divided into $5m \times 5m$ cells partitioned by black plastic curtains to prevent penetration of the light from neighboring cells, with an effective water depth of 4 m. WCDA-1 and WCDA-2, each with an effective area of $150 \times 150m^2$, are equipped with 900 detector units each. On the other hand, WCDA-3, with an area of $300 \times 110m^2$, contains 1320 detector units. For gamma-ray induced showers, WCDA-1 has a threshold of 600 GeV, while WCDA-2 and WCDA-3 have a threshold below 100 GeV due to a modification in the original design. The combination of 8-inch PMT and 1.5-inch PMT pairs has been replaced by the combination of 20-inch and 3-inch PMT pairs. The performance of WCDA-1 was tested by observing the Crab Nebula as a standard candle [10]. The angular resolution of WCDA-1 is approximately 0.45° at 1 TeV and better than 0.2° above 6 TeV. The energy resolution is about 33% for gamma rays around 6 TeV. Considering an aproximate photon acceptance of 50%, the rejection rate of cosmic ray induced showers is about 97.7% at 1 TeV and 99.8% at 6 TeV.

The WFCTA contains 18 Cherenkov telescopes. Each telescope consists of an array of 32 × 32 Silicon photomultipliers (SiPMs), a 5 m^2 spherical aluminized mirror, a power supply system and a slow control system [11]. It has a field of view (FOV) of 16° × 16° with a pixel size of approximately 0.5° × 0.5°. The telescopes are located close to the edges of WCDA pond. WFCTA, WCDA and KM2A can be combined together as a calorimeter-like complex detector to measure air shower energy and composition. For example, all the three array recorded a giant gamma-ray induced shower on 11 January 2020 at 17:59:18 coordinated universal time (UTC), Fig 2. The energy estimated by KM2A and WFCTA is 0.88 ± 0.11 PeV and$0.92^{+0.28}_{-0.20}$ PeV, respectively [12].

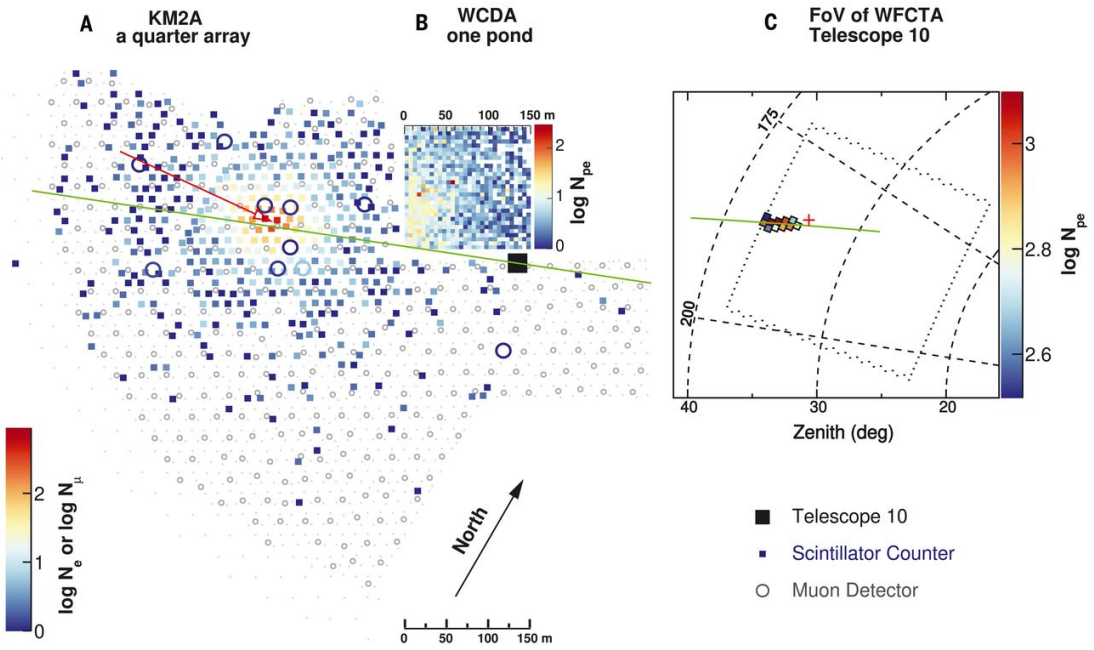

Figure 2: The 0.88-PeV gamma-ray event from the Crab recorded by the LHAASO detectors [12].

3. All Sky survey

With about 400 days of data collected by WCDA and 900 days of data recorded by KM2A, the LHAASO conducted a survey of the northern gamma-ray sky, covering a declination range from −20° to 80° [13]. As a result, a total of 92 sources were observed with an extended size smaller than 2° and a significance above 5.9σ. Among them, 43 gamma-ray sources were detected with UHE emission at a significance level of 4σ, as shown in Fig 3. Most of these UHE sources exhibit higher significance or harder spectral index compared to other sources, indicating that the remaining sources are likely to be detected with UHE gamma-ray emissions as more data is accumulated. This provides important evidence that the Milky Way is rich in UHE sources, which could be associated with pulsars or pulsar wind nebulae, supernova remnants, young massive star clusters, and so on. Further investigations into the spectral and morphological characteristics of these UHE sources are necessary for identification. In section 4, we will present measurements conducted on representative regions.

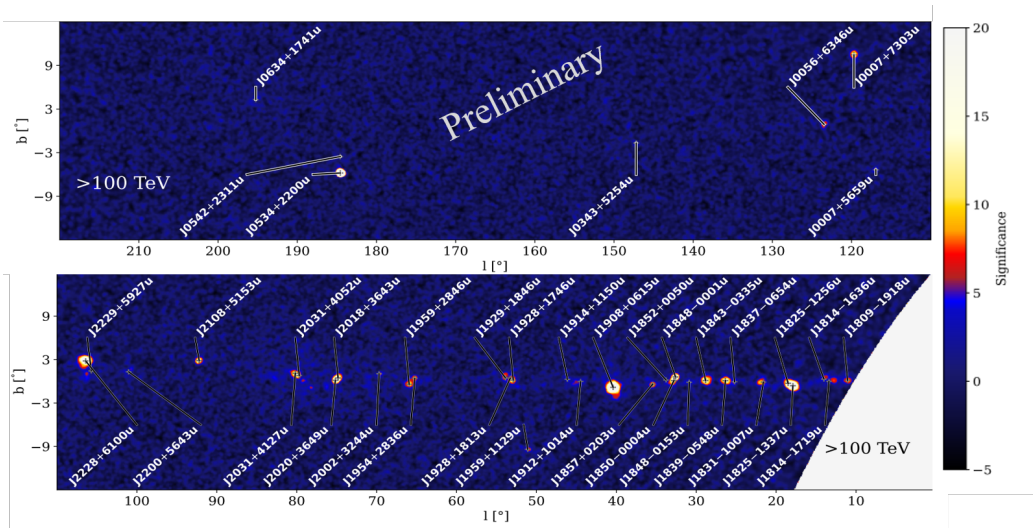

Figure 3: LHAASO significance map with energies above 100 TeV [13].

4. PeVatron Candidates

4.1 Pulsar/Pulsar Wind Nebula

Pulsars are rapidly rotating neutron stars that form after the explosion of a massive star in a supernova event. The strong electric field generated by the rotation of the pulsar is believed to accelerate a relativistic wind of electron-positron pairs, which carries away most of the pulsar's rotational energy and eventually interacts with the surrounding interstellar medium. In this situation, a nonthermal nebula can be formed with the spectrum extends from radio wavelengths to ultra-high energy gamma-rays. In the first LHAASO catalog, a total of 35 sources have been identified as being associated with pulsars, with a chance probability of less than 1% [13]. Fig 4 illustrates the properties of these associated pulsars, highlighting their energetic spindown power and relatively young ages. Among the 35 sources, 22 have been observed as UHE sources. This suggests that PWNe make a significant contribution to the population of UHE sources.

4.1.1 Crab Nebula

The Crab Nebula is the brightest known pulsar wind nebula, powered by the ultrarelativistic electron-positron wind from the pulsar PSR J0534+2200. Serving as a unique cosmic laboratory, the Crab Nebula exhibits an exceptionally broad spectrum of nonthermal radiation that spans an impressive 21 decades of frequencies [14]. This broad-band spectrum displays a distinctive double-peaked structure, following a common characteristic observed in all pulsar wind nebulae. At TeV energies, the Crab Nebula has been observed to have an angular size of approximately 50 arc seconds.

The KM2A data set collected in the operation of half-array for 314 days and three-quarter array for 87 days from December 2019 to February 2021 and 10 months of WCDA-1 data were used to make a dedicated measurement of the Crab Nebula [12]. A total of 89 UHE photons with energy exceeding 100 TeV were detected from the Crab during the time. Two photons with energy of about 0.88 PeV and 1.12 PeV were detected. The energy spectrum was measured from 500 GeV to 1.1

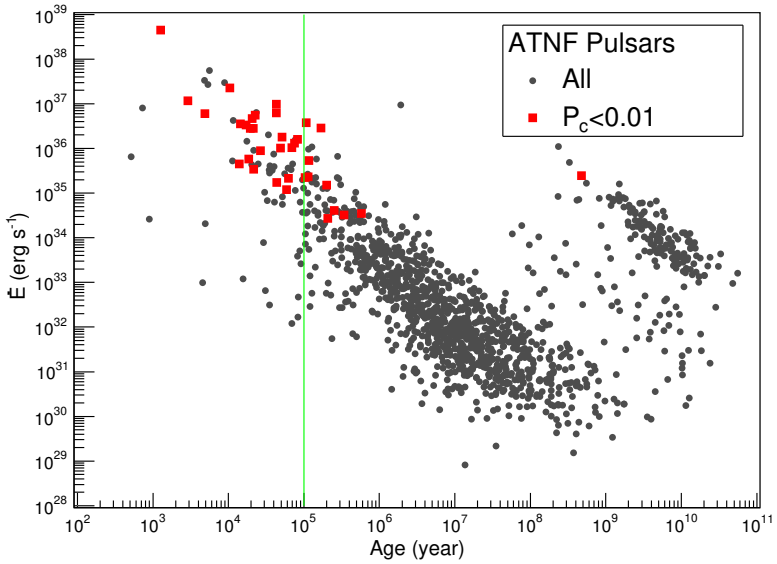

Figure 4: Pulsar spindown power versus age for all pulsars of the ATNF catalog within the FOV of LHAASO [13].

PeV with a spectrum showing gradual steepening over three energy decades. As shown in Fig 5, the fluxes measured by WCDA and KM2A are connected smoothly in the narrow overlapping region around 12.5 TeV. From sub-TeV to multi-TeV, the results of LHAASO are consistent with previous measurements.

The broad-band nonthermal emission of the Crab Nebula can be reasonably explained by the synchrotron radiation and inverse Compton (IC) scattering of relativistic electrons. At energies above 100 TeV, the cosmic microwave background radiation dominates the gamma-ray production and the relation between energies of the photons and the parent electrons is simple. For instance, a photon with an energy of 1.1 PeV corresponds to a parent electron energy of approximately 2.3 PeV. Therefore, the detection of such high-energy photons by LHAASO provides the evidence of a PeV electron accelerator in the nebula. Considering the classical electrodynamics and ideal magnetohydrodynamics theory, it has been found that the acceleration efficiency of electrons in the Crab Nebula can exceed 15% of the theoretical limit. Additionally, the size of the PeVatron is constrained to be between 0.025 and 0.1 parsecs. The spectral points measured by LHAASO below 60 TeV are consistent with the predictions of the one-zone model (as shown in Fig5). However, deviations with a significance of 4σ are observed between 60 and 500 TeV. For more in-depth discussions and analysis, detailed multiwavelength studies can be found in the [12].

4.1.2 PSR J1740+1000

Another interesting UHE source is LHAASO J1740+0948, which is associated with PSR J1740+1000. This pulsar is considered to be middle-aged and is located approximately 1.2 parsecs away from Earth. The pulsar's position is significantly above the Galactic plane, suggesting that it may have originated from a halo-star progenitor. In the X-ray region, an extended and elogated

tail spanning approximately 5.5′ was observed [15]. However, in the TeV energy range, the VERITAS experiment only reported an upper limit of $10^{-13} cm^{-2} s^{-1}$ between 1 TeV and 10 TeV [16]. Additionally, the HAWC detected a faint gamma-ray source with 0.13° away from the PSR J1740+1000.

KM2A analyses this region with approximately 900 days of data [17]. A significant excess, named LHAASO J1740+0948, has been observed in both energy bands of 25 – 100 TeV and > 100 TeV, with significances of h 11.4σ and 5.4σ, respectively. The LHAASO J1740+0948 locate near the extrapolated path of the PWN tail represented by the purple striped line in Fig 6. The source is not significantly extended and the 95% confidence level upper limit is about 0.14°. The energy spectrum of LHAASO J1740+0948 is better described by a logparabola function rather than a simple power-law model. Considering the small extension and large offset, the Pulsar Halo scenario does not seem suitable. If the observed gamma ray emission originates from the pulsar wind nebula tail, the position and offset can be consistently explained.

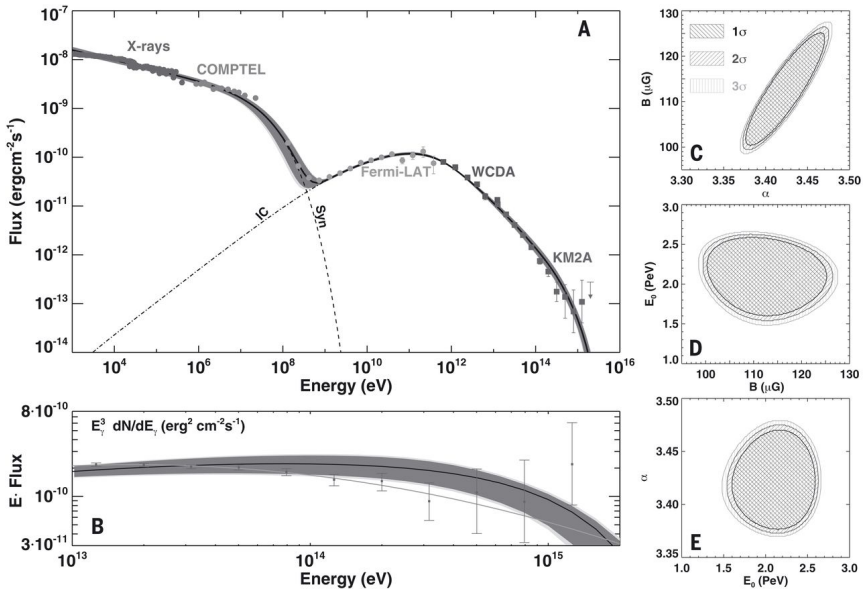

Figure 5: The spectral energy distribution of the Crab Nebula [12].

4.2 Supernova Remnant

Generally, supernova remnants (SNRs) are believed to be the main source of cosmic rays in the Milky Way [18]. There are two main reasons supporting this hypothesis. Firstly, our galaxy experiences approximately three supernova explosions per century, releasing an enormous amount of energy ranging from 10^{50} to 10^{51} ergs. If 10% of this energy is converted into cosmic ray particles, it would provide the necessary energy to sustain the current state of cosmic rays. Secondly, the Diffusive Shock Acceleration (DSA) mechanism offers an efficient way to transfer energy from the explosion's outer shell to cosmic rays, accelerating them to relativistic energies. In 2013, the Fermi observatory detected characteristic decay signals from neutral pions in two middle-aged supernova remnants, IC443 and W44. This direct evidence indicates that SNRs are capable of accelerating

protons to energies in the GeV range. However, further observations and theoretical modeling are still required to determine whether SNRs can accelerate hadronic particles to PeV energies.

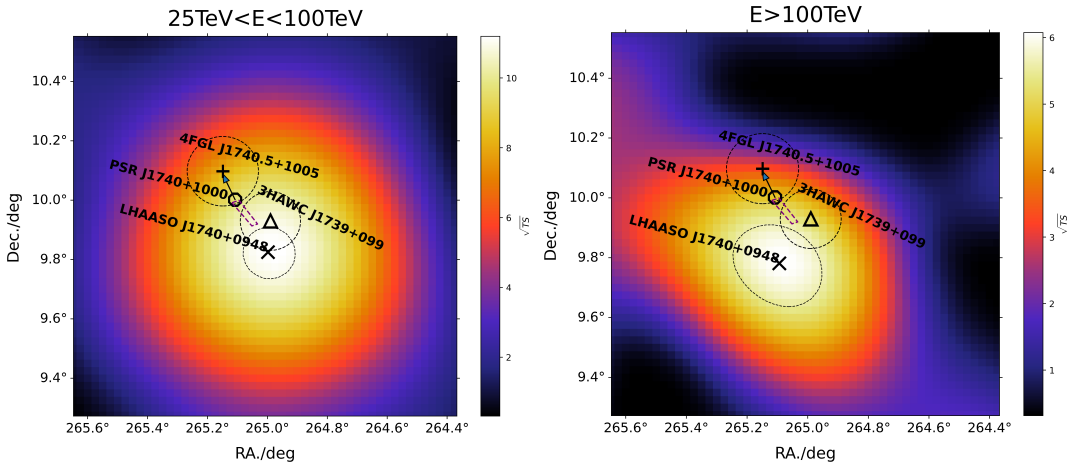

Figure 6: The significance map around LHAASO J1740+0948 region. details can be seen in [17].

4.2.1 W51

W51C is one of the SNRs that has been observed to exhibit a pion zero decay bump [19]. In the case of W51C, the interaction between the expanding shockwave of the supernova remnant and the surrounding molecular clouds leads to the acceleration of cosmic rays. This interaction is supported by the discovery of the 1720 MHz OH maser and the presence of shocked gas in the interaction zone. Many experiments have reported gamma-ray emission in the region.

Recently, a dedicated analysis of this region was conducted by a group from LHAASO [20]. As shown in Fig 7, the LHAASO revealed a significant excess of gamma rays with statistical significances of 17.58σ, 18.37σ, and 5.96σ in three distinct energy ranges: < 25 TeV, 25-100 TeV, and > 100 TeV, respectively. The gamma-ray emission from W51C exhibits an extension of approximately 0.17° ± 0.02° for energies below 25 TeV. However, no significant extension was observed for energies above 25 TeV, with an upper limit of about 0.19° at a 95% confidence level. LHAASO conducted measurements of the differential energy spectrum ranging from 1 TeV to several hundred TeV. It is proposed that the gamma-ray emission is characterized by a power-law function with an exponential cutoff. The observed gamma-ray emission can be explained by high-energy CRs that escaped during the early stages of the SNR, illuminating the adjacent molecular cloud (MC).

4.2.2 SNR G150.3+4.5

LHAASO has also detected UHE gamma-ray emissions in the SNR G150.3+4.5 region [21]. The radio emission from the SNR exhibits a shell-like morphology, measuring approximately 2.5° × 3.0° in size, as depicted in Fig 8. The Fermi-LAT also observed an extended gamma-ray source with a radius of about 1.4°. Below 25 TeV, the gamma-ray emission detected by WCDA is spatially coincident with the radio contours. However, above 25 TeV, the gamma-ray emission detected by KM2A diminishes significantly and appears to be closer to a PSR-like Fermi source.

The energy spectra measured by both WCDA and KM2A can be represented by power laws, but there is a noticeable discrepancy between them due to the significant difference in the sizes of the sources. The challenge lies in determining the origin of the UHE emission, whether it originated from a pulsar or molecular clouds. Two scenarios are discussed in [21].

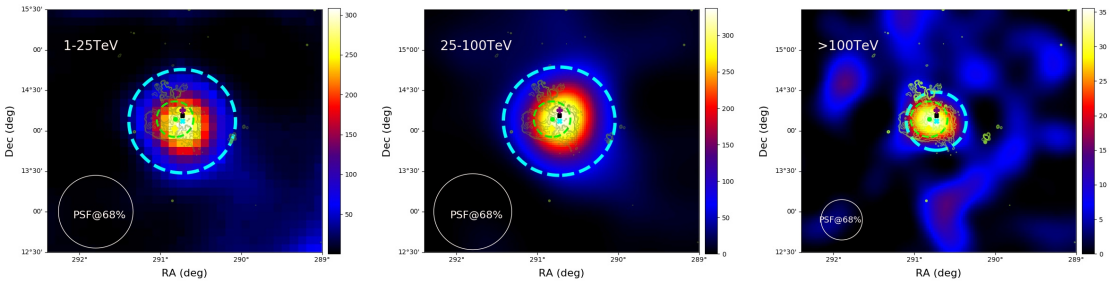

Figure 7: The significance map around W51. The cyan cross and dashed circle are the fitted position and 90% events coverage region of LHAASO [20]. The yellow contours represent the 21 cm radio continuum emission from VLA.

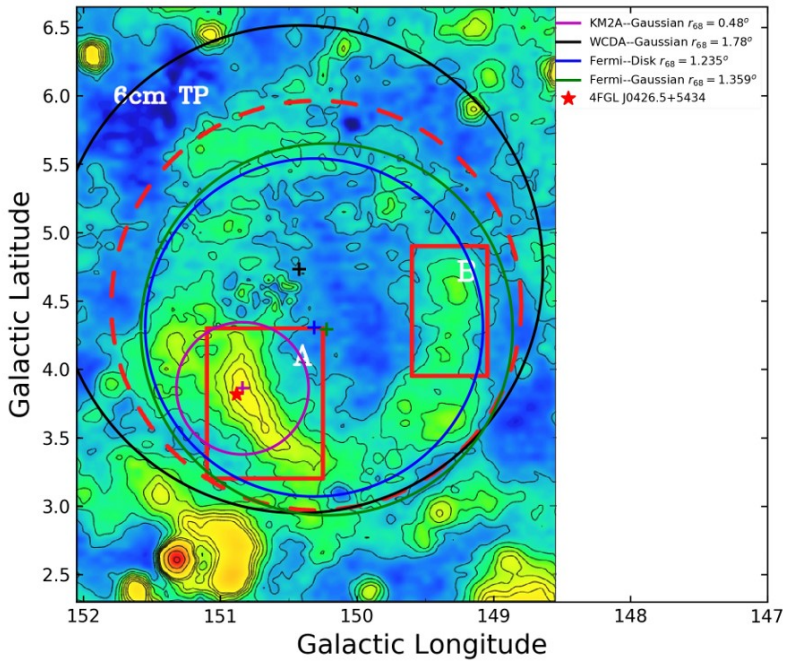

Figure 8: The radio map detected by Urumqi 6 cm observations [21].

4.2.3 SNR G69.7+1.0

The SNR G69.7+1.0 was initially proposed as a SNR in the radio range. However, different experiments have reported varying distances to the SNR from Earth, ranging from 14.4 kpc to 7.8 kpc. In terms of gamma-ray observations, Fermi-LAT is the only instrument that has observed energies lower than 10 TeV. At energies exceeding 25 TeV, LHAASO observed the gamma-ray source appearing as a point-like object [22]. The position of LHAASO is in agreement with the radio and Fermi results, and the energy spectrum exhibits a remarkably hard nature. No significant cutoff was observed before reaching 400 TeV. Currently, the available multiwavelength measurements are insufficient to provide a definitive explanation for the observed phenomena. The data can be accounted for by both leptonic and hadronic models, as shown in Figure 9.

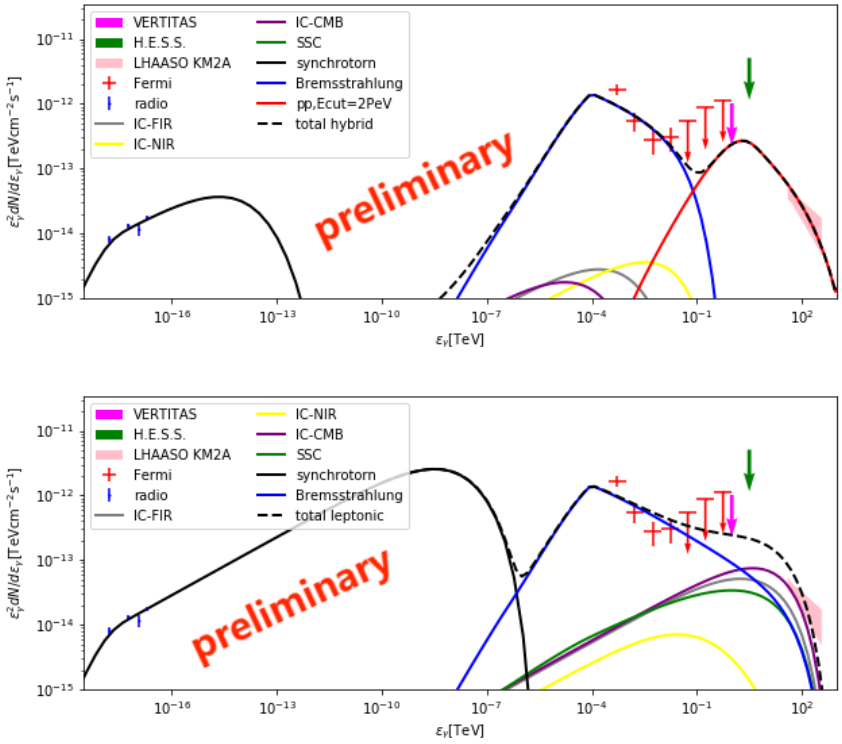

Figure 9: Upper: the multi-wavelength spectrum in the leptonic scenario. Below: the multi-wavelength spectrum in the hybrid scenario [22].

4.3 Star-forming Regions

Star-forming regions are characterized by the presence of young and massive stars, known as OB stars. These stars emit powerful stellar winds, which create shockwaves and turbulence in their surrounding environments [23]. These shockwaves can efficiently accelerate charged particles to relativistic speeds. The Cygnus region, located in the Galactic plane, is famous in the northern sky for the complex features observed across various wavelengths, including radio, infrared, X-rays, and gamma-rays. Situated in the star-forming region of Cygnus X, the Cygnus Cocoon is interpreted

as a cocoon of recently accelerated cosmic rays that are closely associated with the Cygnus superbubble. Recently, LHAASO reported the detection of a photon with energy up to 1.4 PeV in the cocoon region [5]. The measured ratio of muon number (N_μ) to electromagnetic particle number (N_e) for the highest-energy photon is 1/941. This ratio means that nearly all of the CR background is rejected, with an estimated chance probability of 0.028%. With the availability of more data, the Cygnus region was subjected to a detailed analysis, revealing a greater number of photons with energies exceeding 1 PeV. It is evident that the energy spectrum extends beyond the PeV range. Consequently, the results will be published.

LHAASO has the potential to observe interesting star-forming regions, including W43, MC9, RSGC 1, and others. The analysis of these regions is currently in progress, which will contribute to our deeper understanding of the acceleration mechanisms within star-forming regions.

4.4 New UHE Sources

Through the all-sky survey, LHAASO has discovered 32 gamma-ray sources, out of which 13 sources have been detected as ultra-high-energy (UHE) sources [13]. This remarkable achievement opens up the possibility of identifying new candidates for PeV accelerators.

LHAASO J2108+5157 is the first UHE source discovered by LHAASO [24]. No significant counterparts were detected in other wavelengths within the region of LHAASO J2108+5157. While, it is found to be correlated with the molecular cloud [MML2017]4607. The observed UHE gamma rays could potentially be explained by the interactions of protons with the surrounding gas (Fig 10). Other possible scenarios, such as a PWN, can also be invoked to explain the gamma-ray emission. However, no conclusion can be reached regarding the origin of its ultra-high-energy (UHE) emission. The LHAASO J2108+5157 was initially reported as a point-like source with an upper limit of 0.26° at a 95% confidence level (CL). However, with the extensive accumulation of data, the source's extension was observed and the WCDA detected TeV emission from the source. This is beneficial for further identifying and verifying the nature of this source.

5. Galactic Plane Diffuse Gamma-ray

Diffuse gamma-rays are produced through the interactions of cosmic rays with the interstellar medium and radiation fields. They serve as the natural background for a variety of signals. The observation of diffuse emission is vital for accurately detecting gamma-ray sources, whether they are point-like or extended in nature. Additionally, diffuse gamma-rays can be utilized to investigate the spectrum and density of cosmic rays throughout the entire Galaxy.

LHAASO has reported the measurements of diffuse gamma-rays from the Galactic plane between 10 TeV and 1 PeV energies [25]. The inner region ($15° < l < 125°, |b| < 5°$) was detected with a total significance of 29.1σ. On the other hand, the outer region ($125° < l < 235°, |b| < 5°$) was detected with a significance of 12.7σ (see Fig11). This marks the first detection of diffuse emission from 10 TeV to hundreds of TeV in the outer Galactic plane. The fluxes of the diffuse emission in the two regions can be fitted by a power-law function, with an index of -2.99 ± 0.04 for the inner Galaxy region and -2.99 ± 0.07 for the outer Galaxy region. The latitude distributions of the diffuse emission are consistent with the gas distribution. However, there is a noticeable deviation

observed in the longitude distributions. These measurements suggest the presence of additional emission sources or spatial variations in cosmic ray intensities.

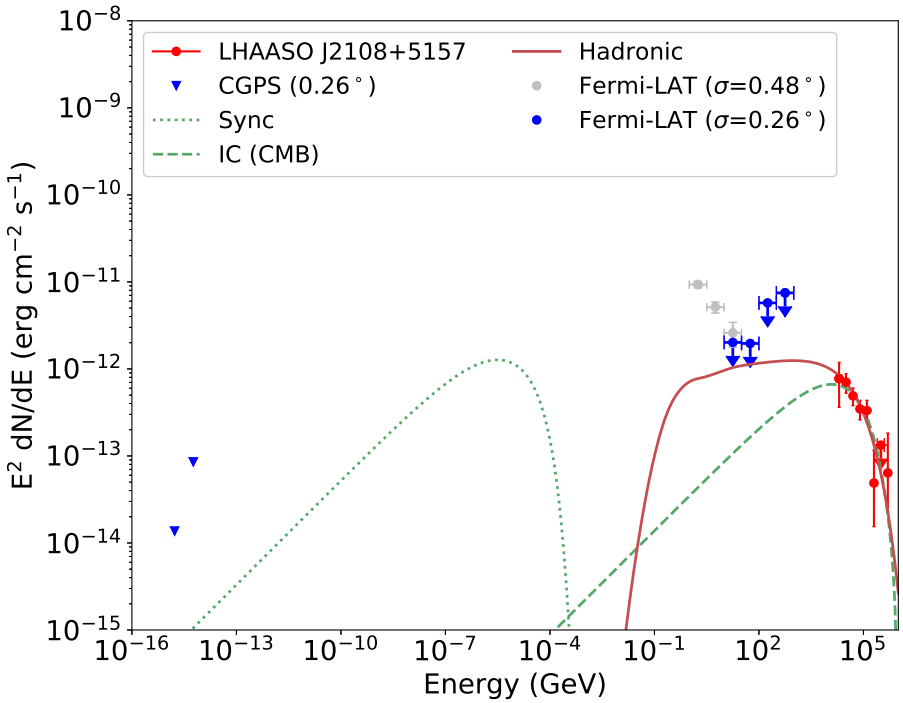

Figure 10: Multiwavelength SED of LHAASO J2108+5157 with hadronic and leptonic models [24].

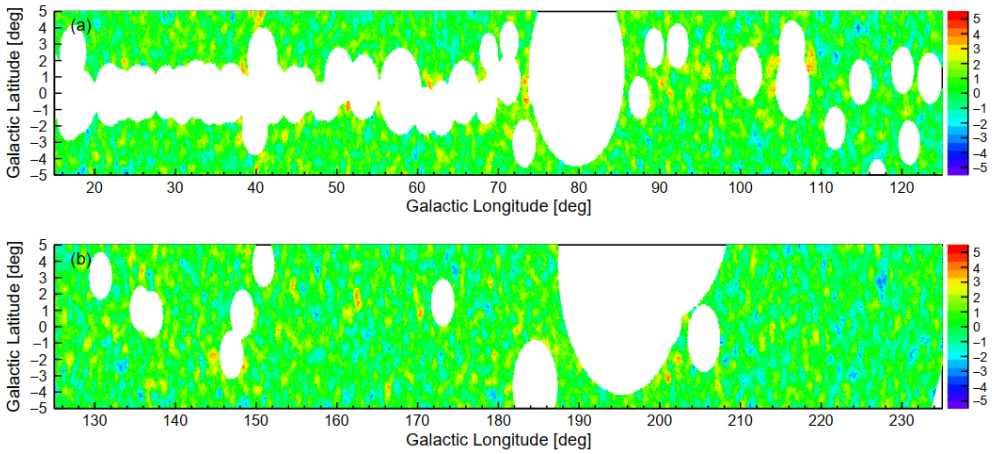

Figure 11: The significance maps in Galactic coordinate of the inner Galaxy region (panel (a)) and outer Galaxy region (panel (b)) above 25 TeV [25].

Acknowledgements

We would like to thank all staff members who work at the LHAASO site above 4400 meters above sea level year-round to maintain the detector and keep the water recycling system, electricity

power supply and other components of the experiment operating smoothly. We are grateful to Chengdu Management Committee of Tianfu New Area for the constant financial support for research with LHAASO data. This work is supported by the following grants: The National Key R&D program of China under grants 2018YFA0404201, 2018YFA0404202, 2018YFA0404203, and 2018YFA0404204, by the National Natural Science Foundation of China NSFC No.12022502, No.12205314, No. 12105301, No. 12261160362, No.12105294, No.U1931201, No. 12005246 and No. 12173039, Youth Innovation Promotion Association CAS No.2022010.

References

[1] Ervin Kafexhiu, Felix Aharonian, Andrew M. Taylor, and Gabriela S. Vila. Parametrization of gamma-ray production cross sections for p p interactions in a broad proton energy range from the kinematic threshold to PeV energies. *PhRvD*, 90(12):123014, December 2014.

[2] M. Amenomori, Y. W. Bao, Bi, and et al. First Detection of Photons with Energy beyond 100 TeV from an Astrophysical Source. *PhRvL*, 123(5):051101, August 2019.

[3] A.U. Abeysekara, A. Albert, Alfaro, and et al. A New Population of Ultra-High-Energy Gamma-Ray Sources Detected by HAWC. September 2019.

[4] Huihai He. Design of the LHAASO detectors. *Radiation Detection Technology and Methods*, 2:7, Jan 2018.

[5] LHAASO Collaboration. Ultrahigh-energy photons up to 1.4 petaelectronvolts from 12 γ-ray Galactic sources. *Natur*, 594(7861):33–36, June 2021.

[6] LHAASO Collaboration. The Large High Altitude Air Shower Observatory (LHAASO) Science Book (2021 Edition). *arXiv e-prints*, page arXiv:1905.02773, May 2019.

[7] Jing Zhao, Jia Liu, Xiang-Dong Sheng, and et al. Design and performances of electromagnetic particle detector for LHAASO-KM2A. *Chinese Physics C*, 38(3):036002, March 2014.

[8] Xiong Zuo, Gang Xiao, Shaohui Feng, and et al. Design and performances of prototype muon detectors of LHAASO-KM2A. *Nuclear Instruments and Methods in Physics Research A*, 789:143–149, July 2015.

[9] LHAASO Collaboration. Observation of the Crab Nebula with LHAASO-KM2A - a performance study. *Chinese Physics C*, 45(2):025002, February 2021.

[10] LHAASO Collaboration. Performance of LHAASO-WCDA and observation of the Crab Nebula as a standard candle. *Chinese Physics C*, 45(8):085002, August 2021.

[11] LHAASO Collaboration. Construction and on-site performance of the LHAASO WFCTA camera. *European Physical Journal C*, 81(7):657, July 2021.

[12] LHAASO Collaboration. Peta-electron volt gamma-ray emission from the Crab Nebula. *Science*, 373:425–430, July 2021.

[13] LHAASO Collaboration. The First LHAASO Catalog of Gamma-Ray Sources. *arXiv e-prints*, page arXiv:2305.17030, May 2023.

[14] MAGIC Collaboration. Observation of Pulsed γ-Rays Above 25 GeV from the Crab Pulsar with MAGIC. *Science*, 322(5905):1221, November 2008.

[15] O. Kargaltsev, Z. Misanovic, G. G. Pavlov, J. A. Wong, and G. P. Garmire. X-Ray Observations of Parsec-scale Tails behind Two Middle-Aged Pulsars. *ApJL*, 684(1):542–557, September 2008.

[16] W. Benbow, A. Brill, Buckley, and et al. A Search for TeV Gamma-Ray Emission from Pulsar Tails by VERITAS. *ApJ*, 916(2):117, August 2021.

[17] Xu RF, Wang K, and LHAASO Collaboration. Possible VHE gamma emission from PWN tail of PSR J1740+1000. In *ICRC2023*.

[18] A. R. Bell. Cosmic ray acceleration. *Astroparticle Physics*, 43:56, March 2013.

[19] T. Jogler and S. Funk. Revealing W51C as a Cosmic Ray Source Using Fermi-LAT Data. *ApJ*, 816(2):100, January 2016.

[20] Fang Kun, Li Zhe, Liu Chen, Chen SongZhan, and LHAASO Collaboration. Detection of Gamma-ray emission from W51 region with LHAASO. In *ICRC2023*.

[21] Zeng Houdun, Guo Yingying, Wu Hanrong, and et al. High energy gamma-ray emission detected by LHAASO from SNR G150.3+4.5. In *ICRC2023*.

[22] Hou BW, Zhang R, Xi SQ, and et al. Discovery of the Ultra-High-Energy gamma-ray source LHAASO J2002+3238 spatially associated with SNR G69.7+1.0. In *ICRC2023*.

[23] Felix Aharonian, Ruizhi Yang, and Emma de Oña Wilhelmi. Massive stars as major factories of Galactic cosmic rays. *Nature Astronomy*, 3:561–567, March 2019.

[24] LHAASO Collaboration. Discovery of the Ultrahigh-energy Gamma-Ray Source LHAASO J2108+5157. *ApJL*, 919(2):L22, October 2021.

[25] LHAASO Collaboration. Measurement of ultra-high-energy diffuse gamma-ray emission of the Galactic plane from 10 TeV to 1 PeV with LHAASO-KM2A. *arXiv e-prints*, page arXiv:2305.05372, May 2023.

Full Authors List: LHAASO Collaboration

Zhen Cao[1,2,3], F. Aharonian[4,5], Q. An[6,7], Axikegu[8], Y.X. Bai[1,3], Y.W. Bao[9], D. Bastieri[10], X.J. Bi[1,2,3], Y.J. Bi[1,3], J.T. Cai[10], Q. Cao[11], W.Y. Cao[7], Zhe Cao[6,7], J. Chang[12], J.F. Chang[1,3,6], A.M. Chen[13], E.S. Chen[1,2,3], Liang Chen[14], Lin Chen[8], Long Chen[8], M.J. Chen[1,3], M.L. Chen[1,3,6], Q.H. Chen[8], S.H. Chen[1,2,3], S.Z. Chen[1,3], T.L. Chen[15], Y. Chen[9], N. Cheng[1,3], Y.D. Cheng[1,3], M.Y. Cui[12], S.W. Cui[11], X.H. Cui[16], Y.D. Cui[17], B.Z. Dai[18], H.L. Dai[1,3,6], Z.G. Dai[7], Danzengluobu[15], D. della Volpe[19], X.Q. Dong[1,2,3], K.K. Duan[12], J.H. Fan[10], Y.Z. Fan[12], J. Fang[18], K. Fang[1,3], C.F. Feng[20], L. Feng[12], S.H. Feng[1,3], X.T. Feng[20], Y.L. Feng[15], S. Gabici[21], B. Gao[1,3], C.D. Gao[20], L.Q. Gao[1,2,3], Q. Gao[15], W. Gao[1,3], W.K. Gao[1,2,3], M.M. Ge[18], L.S. Geng[1,3], G. Giacinti[13], G.H. Gong[22], Q.B. Gou[1,3], M.H. Gu[1,3,6], F.L. Guo[14], X.L. Guo[8], Y.Q. Guo[1,3], Y.Y. Guo[12], Y.A. Han[23], H.H. He[1,2,3], H.N. He[12], J.Y. He[12], X.B. He[17], Y. He[8], M. Heller[19], Y.K. Hor[17], B.W. Hou[1,2,3], C. Hou[1,3], X. Hou[24], H.B. Hu[1,2,3], Q. Hu[7,12], S.C. Hu[1,2,3], D.H. Huang[8], T.Q. Huang[1,3], W.J. Huang[17], X.T. Huang[20], X.Y. Huang[12], Y. Huang[1,2,3], Z.C. Huang[8], X.L. Ji[1,3,6], H.Y. Jia[8], K. Jia[20], K. Jiang[6,7], X.W. Jiang[1,3], Z.J. Jiang[18], M. Jin[8], M.M. Kang[25], T. Ke[1,3], D. Kuleshov[26], K. Kurinov[26,27], B.B. Li[11], Cheng Li[6,7], Cong Li[1,3], D. Li[1,2,3], F. Li[1,3,6], H.B. Li[1,3], H.C. Li[1,3], H.Y. Li[7,12], J. Li[7,12], Jian Li[7], Jie Li[1,3,6], K. Li[1,3], W.L. Li[20], W.L. Li[13], X.R. Li[1,3], Xin Li[6,7], Y.Z. Li[1,2,3], Zhe Li[1,3], Zhuo Li[28], E.W. Liang[29], Y.F. Liang[29], S.J. Lin[17], B. Liu[7], C. Liu[1,3], D. Liu[20], H. Liu[8], H.D. Liu[23], J. Liu[1,3], J.L. Liu[1,3], J.Y. Liu[1,3], M.Y. Liu[15], R.Y. Liu[9], S.M. Liu[8], W. Liu[1,3], Y. Liu[10], Y.N. Liu[22], R. Lu[18], Q. Luo[17], H.K. Lv[1,3], B.Q. Ma[28], L.L. Ma[1,3], X.H. Ma[1,3], J.R. Mao[24], Z. Min[1,3], W. Mitthumsiri[30], H.J. Mu[23], Y.C. Nan[1,3], A. Neronov[21], Z.W. Ou[17], B.Y. Pang[8], P. Pattarakijwanich[30], Z.Y. Pei[10], M.Y. Qi[1,3], Y.Q. Qi[11], B.Q. Qiao[1,3], J.J. Qin[7], D. Ruffolo[30], A. Sáiz[30], D. Semikoz[21], C.Y. Shao[17], L. Shao[11], O. Shchegolev[26,27], X.D. Sheng[1,3], F.W. Shu[31], H.C. Song[28], Yu.V. Stenkin[26,27], V. Stepanov[26], Y. Su[12], Q.N. Sun[8], X.N. Sun[29], Z.B. Sun[32], P.H.T. Tam[17], Q.W. Tang[31], Z.B. Tang[6,7], W.W. Tian[2,16], C. Wang[32], C.B. Wang[8], G.W. Wang[7], H.G. Wang[10], H.H. Wang[17], J.C. Wang[24], K. Wang[9], L.P. Wang[20], L.Y. Wang[1,3], P.H. Wang[8], R. Wang[20], W. Wang[17], X.G. Wang[29], X.Y. Wang[9], Y. Wang[8], Y.D. Wang[1,3], Y.J. Wang[1,3], Z.H. Wang[25], Z.X. Wang[18], Zhen Wang[13], Zheng Wang[1,3,6], D.M. Wei[12], J.J. Wei[12], Y.J. Wei[1,2,3], T. Wen[18], C.Y. Wu[1,3], H.R. Wu[1,3], S. Wu[1,3], X.F. Wu[12], Y.S. Wu[7], S.Q. Xi[1,3], J. Xia[7,12], J.J. Xia[8], G.M. Xiang[2,14], D.X. Xiao[11], G. Xiao[1,3], G.G. Xin[1,3], Y.L. Xin[8], Y. Xing[14], Z. Xiong[1,2,3], D.L. Xu[13], R.F. Xu[1,2,3], R.X. Xu[28], W.L. Xu[25], L. Xue[20], D.H. Yan[18], J.Z. Yan[12], T. Yan[1,3], C.W. Yang[25], F. Yang[11], F.F. Yang[1,3,6], H.W. Yang[17], J.Y. Yang[17], L.L. Yang[17], M.J. Yang[1,3], R.Z. Yang[7], S.B. Yang[18], Y.H. Yao[25], Z.G. Yao[1,3], Y.M. Ye[22], L.Q. Yin[1,3], N. Yin[20], X.H. You[1,3], Z.Y. You[1,2,3], Y.H. Yu[7], Q. Yuan[12], H. Yue[1,2,3], H.D. Zeng[12], T.X. Zeng[1,3,6], W. Zeng[18], M. Zha[1,3], B.B. Zhang[9], F. Zhang[8], H.M. Zhang[9], H.Y. Zhang[1,3], J.L. Zhang[16], L.X. Zhang[10], Li Zhang[18], P.F. Zhang[18], P.P. Zhang[7,12], R. Zhang[7,12], S.B. Zhang[2,16], S.R. Zhang[11], S.S. Zhang[1,3], X. Zhang[9], X.P. Zhang[1,3], Y.F. Zhang[8], Yi Zhang[1,12], Yong Zhang[1,3], B. Zhao[8], J. Zhao[1,3], L. Zhao[6,7], L.Z. Zhao[11], S.P. Zhao[12,20], F. Zheng[32], B. Zhou[1,3], H. Zhou[13], J.N. Zhou[14], M. Zhou[31], P. Zhou[9], R. Zhou[25], X.X. Zhou[8], C.G. Zhu[20], F.R. Zhu[8], H. Zhu[16], K.J. Zhu[1,2,3,6], X. Zuo[1,3]

[1] Key Laboratory of Particle Astrophysics & Experimental Physics Division & Computing Center, Institute of High Energy Physics, Chinese Academy of Sciences, 100049 Beijing, China

[2] University of Chinese Academy of Sciences, 100049 Beijing, China

[3] TIANFU Cosmic Ray Research Center, Chengdu, Sichuan, China

[4] Dublin Institute for Advanced Studies, 31 Fitzwilliam Place, 2 Dublin, Ireland

[5] Max-Planck-Institut for Nuclear Physics, P.O. Box 103980, 69029 Heidelberg, Germany

[6] State Key Laboratory of Particle Detection and Electronics, China

[7] University of Science and Technology of China, 230026 Hefei, Anhui, China

[8] School of Physical Science and Technology & School of Information Science and Technology, Southwest Jiaotong University, 610031 Chengdu, Sichuan, China

[9] School of Astronomy and Space Science, Nanjing University, 210023 Nanjing, Jiangsu, China

[10] Center for Astrophysics, Guangzhou University, 510006 Guangzhou, Guangdong, China

[11] Hebei Normal University, 050024 Shijiazhuang, Hebei, China

[12] Key Laboratory of Dark Matter and Space Astronomy & Key Laboratory of Radio Astronomy, Purple Mountain Observatory, Chinese Academy of Sciences, 210023 Nanjing, Jiangsu, China

[13] Tsung-Dao Lee Institute & School of Physics and Astronomy, Shanghai Jiao Tong University, 200240 Shanghai, China

[14] Key Laboratory for Research in Galaxies and Cosmology, Shanghai Astronomical Observatory, Chinese Academy of Sciences, 200030 Shanghai, China

[15] Key Laboratory of Cosmic Rays (Tibet University), Ministry of Education, 850000 Lhasa, Tibet, China

[16] National Astronomical Observatories, Chinese Academy of Sciences, 100101 Beijing, China

[17] School of Physics and Astronomy (Zhuhai) & School of Physics (Guangzhou) & Sino-French Institute of Nuclear Engineering and Technology (Zhuhai), Sun Yat-sen University, 519000 Zhuhai & 510275 Guangzhou, Guangdong, China

[18] School of Physics and Astronomy, Yunnan University, 650091 Kunming, Yunnan, China

[19] Département de Physique Nucléaire et Corpusculaire, Faculté de Sciences, Université de Genève, 24 Quai Ernest Ansermet, 1211 Geneva, Switzerland

[20] Institute of Frontier and Interdisciplinary Science, Shandong University, 266237 Qingdao, Shandong, China

[21] APC, Universit'e Paris Cit'e, CNRS/IN2P3, CEA/IRFU, Observatoire de Paris, 119 75205 Paris, France

[22] Department of Engineering Physics, Tsinghua University, 100084 Beijing, China

[23] School of Physics and Microelectronics, Zhengzhou University, 450001 Zhengzhou, Henan, China

[24] Yunnan Observatories, Chinese Academy of Sciences, 650216 Kunming, Yunnan, China

[25] College of Physics, Sichuan University, 610065 Chengdu, Sichuan, China

[26] Institute for Nuclear Research of Russian Academy of Sciences, 117312 Moscow, Russia
[27] Moscow Institute of Physics and Technology, 141700 Moscow, Russia
[28] School of Physics, Peking University, 100871 Beijing, China
[29] School of Physical Science and Technology, Guangxi University, 530004 Nanning, Guangxi, China
[30] Department of Physics, Faculty of Science, Mahidol University, 10400 Bangkok, Thailand
[31] Center for Relativistic Astrophysics and High Energy Physics, School of Physics and Materials Science & Institute of Space Science and Technology, Nanchang University, 330031 Nanchang, Jiangxi, China
[32] National Space Science Center, Chinese Academy of Sciences, 100190 Beijing, China